Indian Journal of Engineering & Materials Sciences
Vol. 22, February 2015, pp. 14-22

Effects of Nd/Gd ratio on the microstructures and mechanical properties of Mg-Gd-Y-Nd-Zr alloys

Xuan Liu, Qichi Le*, Zhiqiang Zhang, Lei Bao & Jianzhong Cui

Key Lab of Electromagnetic Processing of Materials, Ministry of Education, Northeastern University, 314Mailbox, Shenyang 110819, People's Republic of China

Received 3 March 2014; accepted 7 October 2014

Three Mg-Gd-Y-Nd-Zr alloys with different Nd/Gd ratios (0.2, 0.5 and 1) are prepared by metal mould casting method. The microstructures and mechanical properties have been investigated. The Nd/Gd ratio has a great influence on the volume fraction of the second phase of the Mg-Gd-Y-Nd-Zr alloys. Volume fraction of the second phase increases with the Nd/Gd ratio increasing. The mechanical properties of the alloys do not get decreased when the Nd/Gd ratio rises up. It should be ascribed to the equal cumulative effect of solid solution strengthening and second phase strengthening. The as-extruded Mg-6Gd-3Y-6Nd-0.6Zr has the best mechanical properties and lowest Gd addtion, and its ultimate tensile strength, yield strength and elongation are 336 MPa, 300 MPa and 2.5%, respectively.

Keywords: Mg-Gd-Y-Nd-Zr alloy, Microstructure, Inverted extrusion, Mechanical properties

Due to the restriction of resource and energy, the lightening of material becomes a key factor in developing new materials. Magnesium alloys, as the lightest structural material, get highly focused on due to their high specific strength, specific stiffness and good cast-ability[1]. However, the application of the Mg alloys is still limited, due to their poor mechanical properties, especially at the elevated temperature[2,3].

Magnesium alloys with RE (rare earth element) addition, are known for the excellent performance at the elevated temperature as well as room temperature, owing to the formation of heat-resistant compounds with high strength[4-6]. The RE could be divided into light RE (La, Ce, Pr, Nd. etc.) and heavy RE (Gd, Tb, Dy, Ho, etc.). Magnesium alloys with heavy RE such as Mg-Gd based alloys with Gd addition over 10 wt%, have been extensively studied for their potential in achieving higher strength and better creep resistance[7,8]. It was demonstrated recently that an appreciably high 0.2% proof strength of 445 MPa could be achieved in a Mg-14 wt% Gd-0.5 wt% Zr alloy produced by the combined processes of hot extrusion, cold work, and aging[9]. However, large amount of Gd is required for Mg alloys to achieve the high strength[10], which bring the problem that the densities of these Mg alloys would be much larger than those of commercial magnesium alloys. It partially sacrifices the advantage of lightness for magnesium alloys.

The densities of Nd and Y are lower than those of Gd. What's more, among Mg-light RE binary alloys, Mg-Nd alloys show a higher strength for a high equilibrium solid solubility[11]. Meanwhile, it was reported that Nd addition in Mg-Gd based alloys could improve the mechanical properties and the aging responses[12,13]. It was also reported that Y addition in Mg-Gd based alloys could refine the grains and improve the aging response of Mg-RE alloys[14,15]. Thus, on the consideration of the low density, the approach to improving the strength of Mg-RE alloys should be making use of optimum combinations and additions of light and heavy rare earth elements, instead of increasing the heavy RE addition; and quaternary Mg-Gd-Y-Nd-Zr alloys with certain additions might be an efficient way to improve the strength[16,17].

In this study, three Mg-Gd-Y-Nd-Zr alloys with different Nd/Gd ratios were prepared, aimed at obtaining high strength and low density Mg-Gd based alloys by substituting a part of Gd with Nd. The effects of Nd/Gd ratio on the microstructure and mechanical properties of the as-cast and as-extruded alloys are being investigated. The relationship between the microstructures and the mechanical properties will also be discussed.

*Corresponding author (E-mail address: qichi1@mail.neu.edu.cn).

Experimental Procedure

This work adopts high purity elemental Mg (>99.95%), Mg-25Gd (wt%), Mg-50Y (wt%), Mg-25Nd (wt%) and Mg-30Zr (wt%) master alloy as the raw material. The alloys were melted in a mild steel crucible, and heated in an electric resistance furnace. Flux was used to purify the melt, as well as prevent from burning. The melt was kept at 983 K for 10 min, and then poured into a preheated steel mould. The casting ingots were 60 mm in diameter and 120 mm in height. The compositions of the alloys were obtained by chemical analysis and listed in Table 1. Homogenization treatment was carried out at 783 K for 16 h. After homogenization, the ingots were machined into Φ47 mm cylinders with a length of 100 mm, and were indirectly extruded into Φ12 mm rods with a speed of 5.6 cms^{-1} in a Φ50 mm extruding container, at 673 K. Meanwhile, the extrusion ratio was 15:1, and the container and mould were preheated to 523 K. Then the rods were machined into tensile specimens of 6 mm gauge diameter and 25 mm gauge length, according to the ASTM standard B557M-10. The tensile direction was parallel to the extrusion direction. Tensile test was performed by universal tensile testing machine (the speed of tensile was 1 mm/min) at room temperature (RT).

Microstructures were observed by optical microscope (OM), transmission electron microscope (TEM) and scanning electron microscope (SEM) coupled with an energy dispersive X-ray analyzer (EDX). The phase analysis were performed with an X-ray diffractometery (XRD). Linear intercept method was applied to determine the grain size of the alloys. Volume fraction of phases were estimated by image analysis technique using at least ten areas for each alloy. Vickers hardness testing was carried out by 10 kg load for 20 s.

Result and Discussion

Microstructures of the alloys in as-cast and as-homogenized condition

Figure 1 shows the microstructures of the alloys in as-cast and as-homogenized condition. It implies that the as-cast alloys are mainly composed of α-Mg and large amount of discontinuous eutectics at the triple points of grains. However, the RE addition of the investigated alloys are much lower than the eutectic point of Mg-Gd (9.48 at%), Mg-Y (9.01 at%) and Mg-Nd (7.66 at%), respectively. It should be ascribed to the non-equilibrium solidification caused by the fast cooling rate of commercial casting processes[18]. If one assumes no diffusion in the solid but perfect mixing in the liquid, the mean composition of the solidifying α-Mg crystals is always lower than the nominal composition of the alloy. As a consequence, the liquid becomes increasingly enriched in solute and finally solidifies as eutectic consisting of β phases and α-Mg solid solution at T_E. Grain size of the as-cast alloys is about 20~30 μm, and it isn't influenced by Nd/Gd ratios. After homogenization at 783 K for 16 h, the grain size of the alloy increases slightly, and a certain quantity of second phase are unable to resolve into the matrix, as shown in Fig. 1 (b), (d) and (f).

Figure 2 shows the volume fraction of the eutectic phase and undecomposed second phase in the as-cast and as-homogenized alloys, respectively. Volume fraction of the eutectic phases in the as-cast alloys increases with the increasing Nd/Gd ratio. It should be ascribed to the low Nd solubility[19]. After homogenization, volume fraction of the undecomposed second phase is also increase with the Nd/Gd ratio.

Figure 3 shows the Vickers hardness of the as-cast alloy. The results indicate that the as-cast specimens' Vickers hardness are free from the effect of Nd/Gd ratio. The strengthening mechanisms are mainly solid solution strengthening, refined crystalline strengthening and second phase strengthening[20]. Firstly, the microhardness values of the matrix show that the solid solution strengthening effect are identical in the investigated as-cast alloys. Secondly, refined crystalline strengthening effect should be the same on account of the similar grain size. Thus, it can be concluded that the increasing grain boundary eutecitc could not promote the hardness of the as-cast alloys.

Figure 4 shows the XRD patterns of the alloys in as-cast and homogenized conditions. The as-cast alloys are mainly composed of α-Mg and Mg_5(GdYNd),

Table 1 – Chemical compositions of investigated alloys

Alloys	Nominal composition	Gd	Y	Nd	Zr	Fe	Pb	Mg
1	Mg-10Gd-3Y-2Nd-0.6Zr	11.0	3.05	1.87	0.34	0.021	0.004	Bal
2	Mg-8Gd-3Y-4Nd-0.6Zr	7.74	3.2	3.96	0.34	0.015	0.025	Bal
3	Mg-6Gd-3Y-6Nd-0.6Zr	6.07	2.17	6.48	0.31	0.014	0.043	Bal

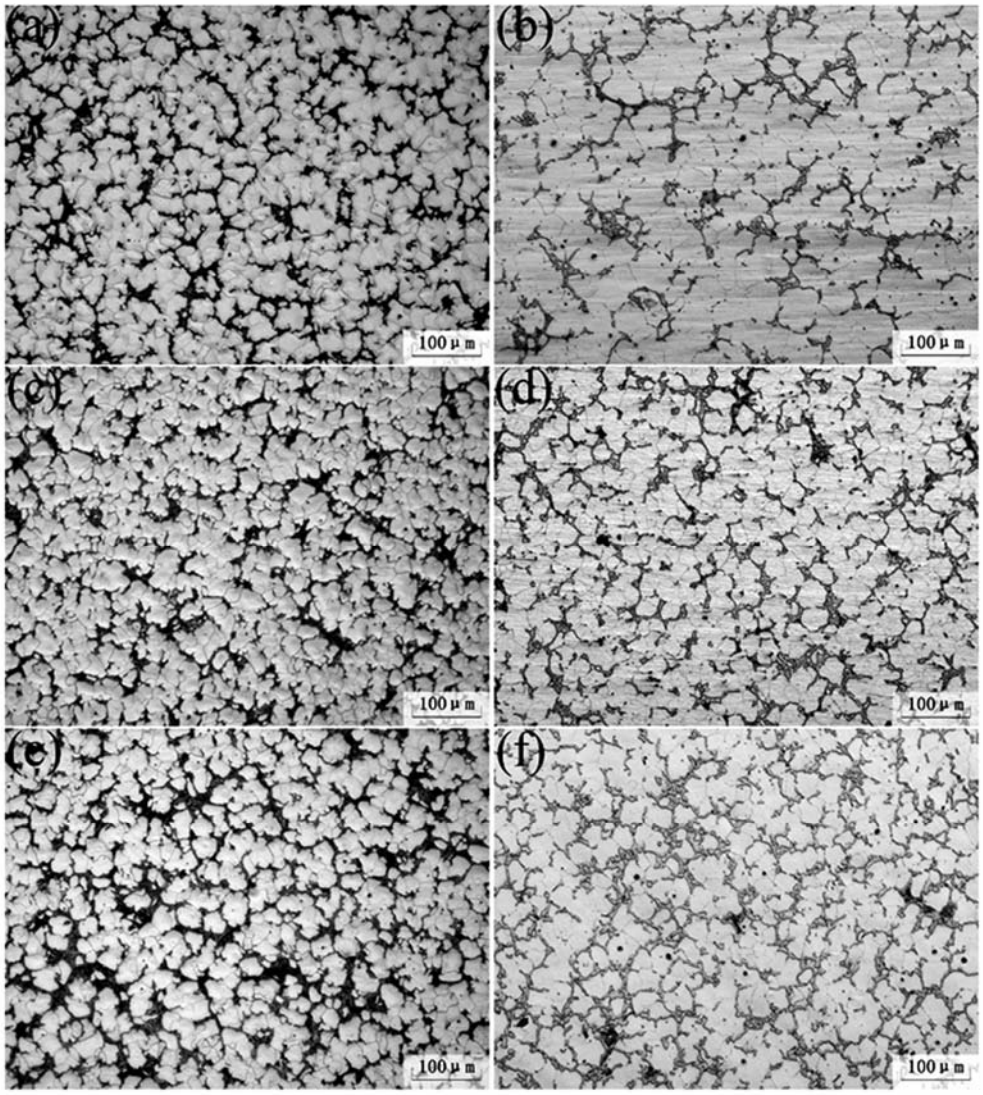

Fig. 1 – Optical images of the as-cast and as-homogenized specimens (a, b) Alloy 1; (c, d) Alloy 2; (e, f) Alloy 3 (a, c and e as-cast; b, d and f as-homogenized)

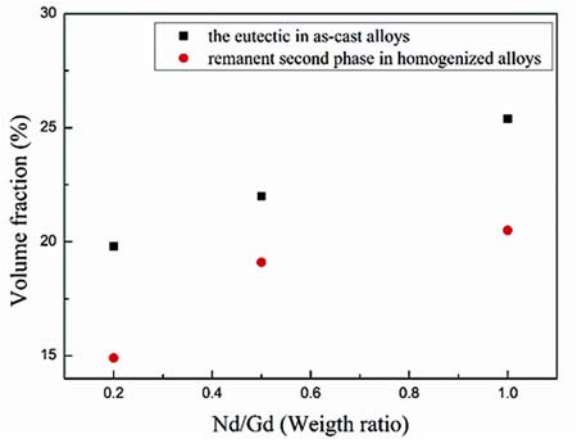

Fig. 2 – Volume fraction of the second phase in the as-cast and homogenized alloys

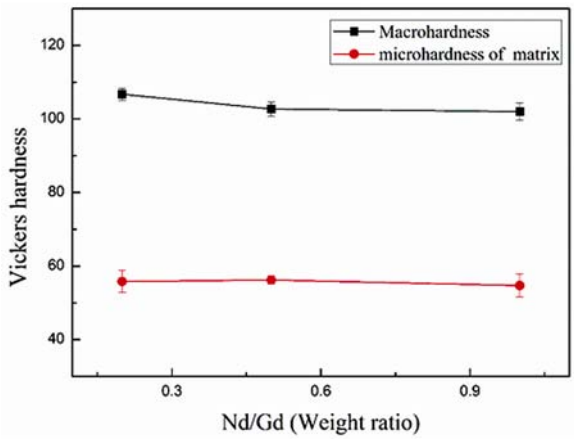

Fig. 3 – Vickers hardness of the matrix and second phase in the as-cast alloys

where Y and Nd element probably substitute for Gd element. It is widely reported that Gd element are substituted by other RE in the second phase[21,22]. With the augment Nd/Gd ratio, no obvious diffraction peaks for $Mg_{41}(NdYGd)_5$ are figured out in the as-cast Alloy 3. However, Fig. 4(b) shows that the amount of $Mg_{41}(NdYGd)_5$ is increasing in the as-homogenized Alloy 3. The phase composition of as-homogenized Alloy 3 is mainly α-Mg, $Mg_5(GdYNd)$ and $Mg_{41}(NdYGd)_5$. It can be concluded that phase composition has been influenced by the Nd/Gd ratio after homogenization, which will be discussed in detail later. Meanwhile, a new phase is found in the homogenized XRD pattern, represented by the rhombus, as shown in Fig. 4. It was supposed to be the cuboid phase with a fcc structure after solid solution or homogenization[23].

Figure 5 and Table 2 show the SEM images and corresponding EDS results of Alloy 1 and Alloy 3 in the as-cast and homogenized conditions.

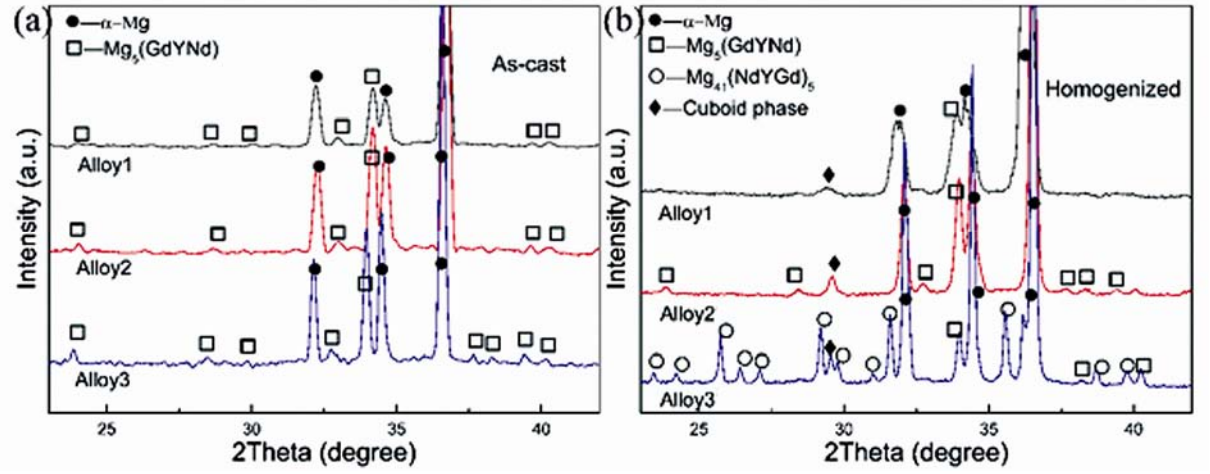

Fig. 4 – X-ray diffraction patterns of the as-cast and as-homogenized alloys (a) as-cast alloys and (b) as-homogenized alloys

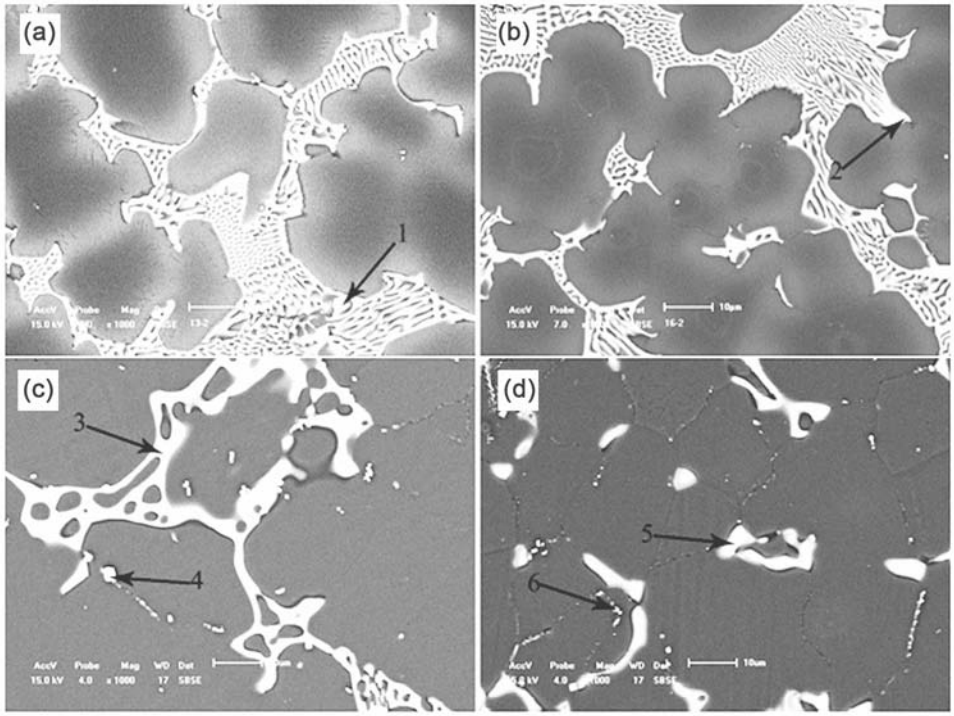

Fig. 5 – SEM images of as-cast and as-homogenized alloys (a) and (c) as-cast and as-homogenized Alloy 1, respectively; (b) and (d) as-cast and as-homogenized Alloy 3, respectively

Table 2 – Corresponding EDS results in Fig. 5

Point	Mg, at%	Gd, at%	Y, at%	Nd, at%
1	87.68	5.62	3.44	3.26
2	86.87	2.01	2.32	8.80
3	86.36	7.56	2.56	3.52
4	63.38	11.34	25.08	0.20
5	89.94	2.58	0.71	6.77
6	78.07	6.01	14.39	1.53

Morphologies of the second phases change from eutectics to dissociative bulk and cuboid phases, as shown in Fig. 5. The SEM images seemingly indicate that the volume fraction of the remnant second phase in as-homogenized Alloy 1 (Fig. 5c) seems to be more than that in as-homogenized Alloy 3 (Fig. 5d). Figure 5 is going for the clear observation and accurate EDS analysis in a large magnification (1000×) avoiding the interference from the matrix, but these local microareas could not represent the whole area of the alloys. EDS of point 1 and 2 suggest that the white eutectic distributed along the grain boundaries should be Mg_5(GdYNd) in Fig. 5(a) and (b). It has been reported in Mg-Gd-Y-Nd alloys that these eutectics are $Mg_5(Gd_{1-x-y}Y_xNd_y)$ compound[21]. The key point is, eutectic in Alloy 1 and Alloy 3 keep different content of Nd and Gd. In other words, compositions of the Mg_5(GdYNd) are effected by the Nd/Gd ratios of the alloys. EDS results of point 5 suggests that $Mg_{41}(NdYGd)_5$ has been found in the as-homogenized Alloy 3. Because the atomic ratio between Mg and RE of the phase is approximately 8:1. It also suggests that the amount of $Mg_{41}(NdYGd)_5$ in Alloy 3 increases after homogenization. The results are in good agreement with the XRD patterns.

Then, the phase composition for the as-cast and as-homogenized Alloy 3 is discussed. It is identical for the alloy constituent of Nd and Gd in Alloy 3, and EDS result of the as-cast Alloy 3 indicates that the amount of un-dissolved Nd is more than that of Gd. However, the primary second phases are Mg_5(GdYNd) rather than $Mg_{41}(NdYGd)_5$. It should be attributed to the solute concentration of the liquid upon the precipitation of eutectics in the solidification process as well as the element electronegativity difference. It has been mentioned above that the conventional casting are common non-equilibrium solidification. During the solidification process, most of the solute are pushed into the liquid upon solid liquid interface. At the final stage, the solute concentration of the remnant liquid are high and close to the eutectic point of Mg-Gd, which are speculated through the XRD patterns in Fig. 4. Thus, the nucleation and growth of β-Mg_5Gd are synchronous with those of α-Mg. On the other hand, it should be noted that the difference in electronegativity between Mg and Gd is larger than that between Mg and Nd, because the positional difference among Mg and Gd is larger in the periodic table. Due to the larger electronegativity difference, Gd atoms are prior to bond with Mg, forming the compound Mg_5Gd, although the amount of unresolved Nd is more than that of Gd. What's more, the amount of liquid decreases with the solidification further in progress, due to the synchronous nucleation and growth of α-Mg and β-Mg_5Gd at the final solidifying stage. There are no sufficient Mg atoms for Nd and Y atoms to combine with, forming $Mg_{41}Nd_5$ or $Mg_{24}Y_5$. On the basis of the SEM and EDS result, it is quite possible that Nd and Y atoms participate in the formation of Mg_5Gd by substituting for Gd atoms, owing to the chemical similarity of RE element. As a consequence, it is reasonable that Mg_5(GdYNd) become the primary second phase in the as-cast Alloy 3.

After homogenization, the formation of $Mg_{41}(NdYGd)_5$ in Alloy 3 could be observed in the XRD pattern and EDS analysis. Concentration gradient should be the primary force to drive Gd, Y and Nd from the second phase to the α-Mg during the homogenization. To the best of our knowledge, the largest solid solubility of Gd and Nd in Mg are 23.3 wt% and 3.6 wt%, respectively and the Mg_5(GdYNd) compounds are not very stable at the homogenization temperature[19]. For Alloy 3, the Nd addition of 6 wt% exceed the largest solid solubility. Thus, Nd element could be partially resolved into the matrix during homogenization. With the progressing decomposition of Mg_5(GdYNd), most of Gd element are resolved into the matrix, due to the sufficient driving force. As a consequence, in the investigated homogenization process, the unresolved Nd element could have opportunity to combine with Mg, forming $Mg_{41}(NdYGd)_5$, where the unresolved Gd and Y substitute for Nd element. This is the reason why the amount of $Mg_{41}(NdYGd)_5$ is increasing in the as-homogenized Alloy 3.

In addition, similar cuboid phases were also observed in the as-homogenized alloys[24]. They are supposed to be the last product before the Mg_5(Gd, Y, Nd) phases are completely dissolved into the matrix, which is in agreement with the results in reference[25]. EDS of point 4 and 6 indicate that the cuboid phases

are rich in Y and Gd but poor in Nd. It is possibly related to the fact that Y is a surface-active element to Mg[14]. Analogous cuboid phase is also found in Mg-10Gd-2Y-0.5Zr alloy after solution treatment, and its formation mechanism is reported as well[24].

Microstructures of hot extruded alloys

Figure 6 shows the OM images of the as-extruded alloys. The undecomposed second phases are cracked, distributing along the extrusion direction, like strips. It suggests that these second phases are poor in plasticity. It could clearly show from Fig. 6(b), (c) and (d) that the space between these the cracked second phase strips decreases with the increasing Nd/Gd ratio. That is to say, the number density of the cracked second phase increases with the increasing Nd/Gd ratio. As discussed in the homogenization process, the amount of the undecomposed second phase is augment with the increasing Nd/Gd ratios. Therefore, it is reasonable that number density of these 'strips' increase with the augment Nd/Gd ratio. Meanwhile, dynamic recrystallization (DRX), is also observed in the microstructures of all three as-extruded alloys, and the recrystallized grains of the three alloys are all well refined. It suggests that the Nd/Gd ratio has little influence on the DRX process. Grain size inhomogeneity is also observed in Fig. 6(a). It indicates that the cracked phase could have a significance effect on the nucleation and growth of DRX grains.

Figure 7 shows the XRD patterns of the as-extruded alloys. It could be seen that the phase composition of the Alloy 3 is mainly α-Mg, $Mg_5(GdYNd)$ and $Mg_{41}(NdYGd)_5$. The phase composition are close to those of the as-homogenized alloys.

Figure 8 and Table 3 show the TEM images and corresponding EDS results of the alloys in extruded condition. EDS of point 7 suggests that the bulk phase

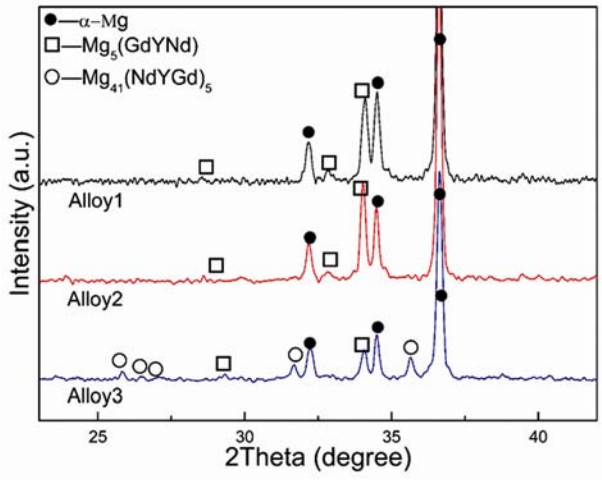

Fig. 7 – XRD patterns of the as-extruded alloys

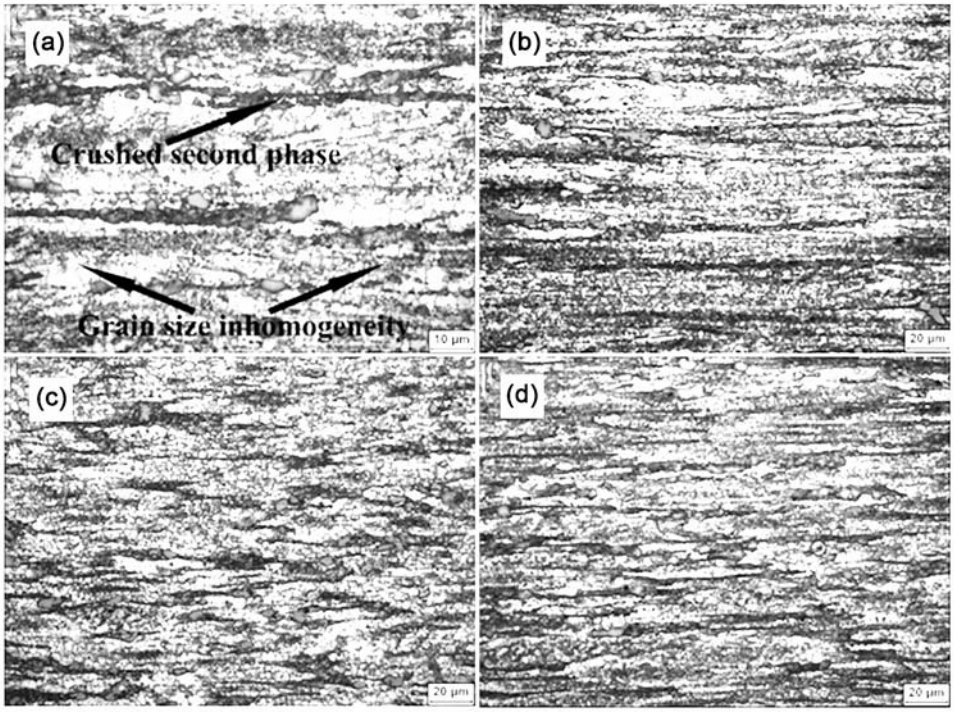

Fig. 6 – The Optical micrographs of as-extruded alloys (a) and (b) Alloy 1, (c) Alloy 2, (d) Alloy 3

of Alloy 1 in Fig. 8(a) is confirmed as $Mg_5(GdYNd)$. Points 9 and 11 indicate that there are two kinds of cracked second phases in the as-extruded Alloy 3. The phase represented by point 9 has the Mg:RE atomic ratio of 8:1, so it is identified as $Mg_{41}(NdYGd)_5$. The atomic ratio between Mg and RE of point 11 is approximately 5:1, thus it is confirmed as $Mg_5(GdYNd)$. The two kinds of second phase are completely consistent with the XRD pattern in Fig. 7.

Figure 8(c) shows that the dislocations pile up around the second phases. A mismatch between the deforming ability of Mg matrix and secondary phase brings about stress concentrations, promoting the dislocation movement. However, during the hot extrusion, the crushed second phases become obstacles against the movement of dislocations, bringing in dislocations piling up, as shown in Fig. 8(c). Meanwhile, RE addition could decrease the stack-fault energy of the alloys[26]. It is difficult to free dislocations from the dislocation networks. Therefore, the density of the dislocations is increasing during extrusion, which can introduce a higher driving force for nucleation and growth of recrystallized grains[27]. To further reduce the stress concentration, the pile-up dislocations around the grain boundaries and the cracked second phases rearrange themselves to form groups of low angle boundaries, which lead to the development of subgrains or substructures, as illustrated in the previous report[28]. Meanwhile, Fig.8(f) shows that the recrystallized grain boundaries are surrounded by the crushed second phases and some dislocations could also be observed around the grain boundary, suggesting that the cracked second phase could indeed restrain the movement of recrystallized grain boundaries[8]. Thus, fine recrystallized grains are obtained by hot extrusion. What's more, the grain refinement is attributed to the high nucleation rate of DRX grains induced by the mechanism known as particle-stimulated nucleation (PSN)[29] at the interfaces between precipitates and the matrix, and the precipitates could suppress the growth of DRX grains. The PSN mechanism involves a rapid subgrain boundary migration in the deformation zone around large hard particles during extrusion[28]. The accumulation of misorientation by the rapid subgrain boundary migration could generate high-angle grain boundaries. Due to the uneven distribution of the second phases, the deformation or dislocations accumulation is not uniform, resulting in inhomogeneity of DRX grains, as shown in Fig. 6(a).

In addition, certain quantity of particle phase is discovered, as shown in Fig. 8(a) and (d). EDS analysis of spot 8 and 10 indicate that about 3 at% Pb

Table 3 – Corresponding EDS results in Fig. 8

Point	Mg, at%	Gd, at%	Y, at%	Nd, at%	Fe, at%	Pb, at%
7	82.99	9.81	3.64	3.01	0.54	-
8	93.90	1.55	0.52	0.33	0.53	3.18
9	88.92	3.05	1.35	7.68	-	-
10	94.33	0.86	0.64	0.32	0.61	3.25
11	85.63	5.38	2.51	5.62	0.87	-

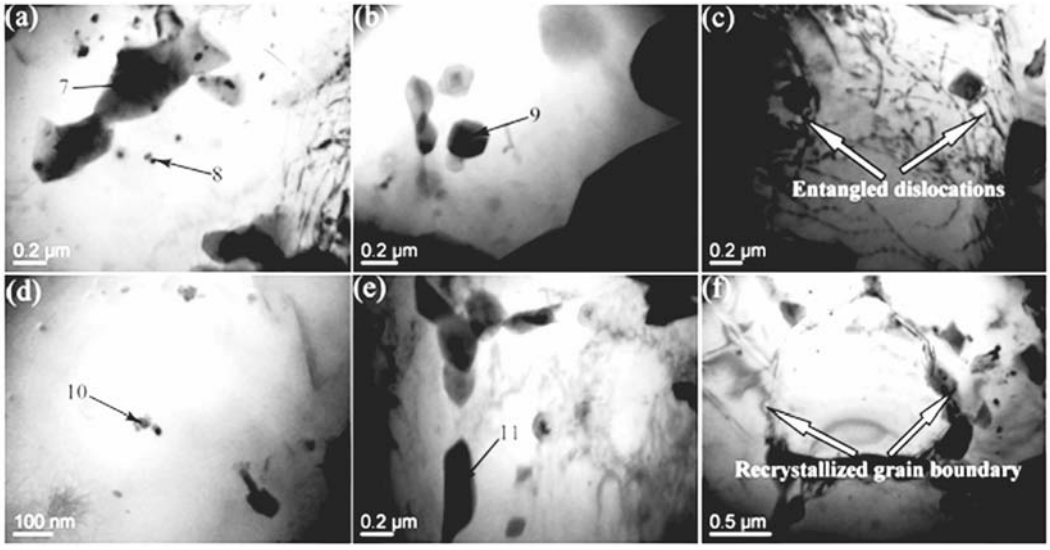

Fig. 8 – TEM images of the as-extruded alloys (a) as-extruded Alloy 1; (b), (d) and (e) extruded Alloy 3; (c) dislocations in the as-extruded Alloy 1; (f) recrystallized grain in the as-extruded Alloy 1

are contained in these particle phases. These precipitations are seem to be different from those reported in Refs[16,30,31], because the content of RE is low in the particles. The formation of these particle phases should be attributed to the dynamic precipitation[28,32] The supersaturated α-Mg solid solution offers concentration gradient for dynamic precipitation. Furthermore, high density dislocations and vacancies are formed during hot deformation, which provided a high diffusion path for solute elements. Therefore, these particles tend to precipitate, and they can further bring about additional barriers to the movement of dislocation, resulting in the accumulation of dislocation and the formation of subgrains[31]. On the other hand, the piling dislocations provide driving force and positions for nucleation of dynamic precipitation in the extruding process[33]. Thus, these dynamic precipitates in the matrix could also restrain the movement of dislocations as the cracked second phase do, which could also refine the microstructures.

It is reported in the previous literatures that dynamic precipitation could retard dynamic recrystallization, due to the comptition between dynamic precipitation and DRX[16,34]. In this work, dynamic precipitation doesn't occur drastically, not strong enough to restrain the DRX process. Consequently, dynamic precipitation and DRX occur at the same time.

Mechanical properties

The mechanical properties including ultimate tensile strength (UTS), tensile yield strength (TYS) and elongation (ε) of the as-extruded alloys at room temperature are summarized in Fig. 9. UTS and TYS of the extruded Alloy 1 are 333 MPa and 299 MPa, respectively. Compared to Alloy 1, UTS and TYS of Alloy 2 have a slight decrease of about 20 MPa. UTS and TYS of Alloy 3 are approximately identical to those of Alloy 1. It could be seen that the strength does not change substantially by replacing a part of Gd with Nd.

The number density of the second phase increases with the increasing Nd/Gd ratio. It was reported that the cracked second phase could restrain the movement of recrystallized grain boundaries and dislocations[8,28]. The harder second phase is probably contributing to the increasing of strength, due to precipitate strengthening by the Orowan mechanism[30]. On account of the similar recrystallized grain size, it suggests that the cumulative effect of solid solution strengthening and the second phase strengthening are close for the three as-extruded alloys. The slight strength decrease in Alloy 2 should be related to the distributing condition of the cracked phases, as shown in Fig. 6(c). It should be concluded that mechanical properties of the extruded alloys are not decreasing with the increasing Nd/Gd ratios. However, the densities of the alloy decrease with the increasing Nd/Gd ratios, due to the reduced Gd addition.

Figure 10 shows that the fracture surface of the extruded alloys is very flat and cleavages can be

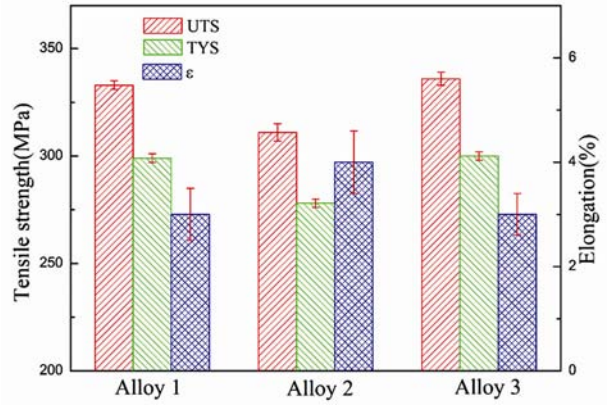

Fig. 9 – Mechanical properties of the as-extruded alloys at room temperature

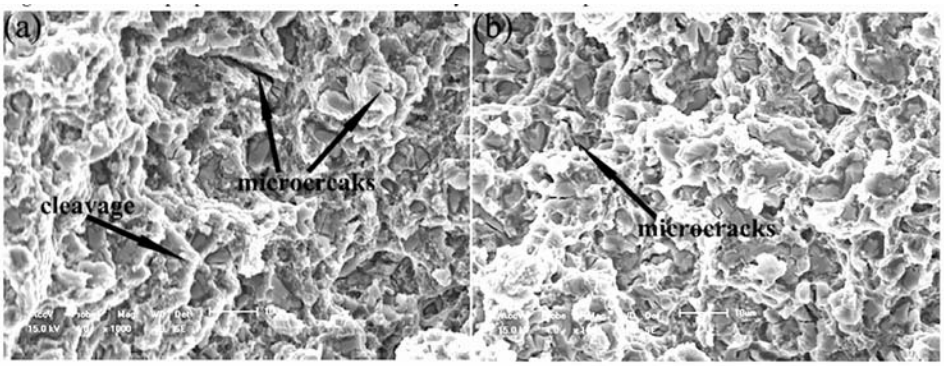

Fig. 10 – Typical fracture surface image of the as-extruded alloys (a) Alloy 1; (b) Alloy 3.

observed. Stress concentration is easily achieved by the brittle second phase, causing microcracks. Elongations of the extruded are very small due to the suppression of dislocations mobility by these second phase particles.

Conclusions

In this study, the best mechanical properties are obtained from the extrueded Mg-6Gd-3Y-6Nd-0.6Zr alloy with the lowest Gd addition, and the ultimate tensile strength, yield strength and elongation are 336 MPa, 300 MPa and 2.5%, respectively. Microstructures of the Mg-Gd-Y-Nd-Zr alloys have been also investigated. The as-cast Mg-Gd-Y-Nd-Zr alloys mainly consist of α-Mg and Mg_5(GdYNd). The primary phase composition of the as-cast alloys aren't influenced by the Nd/Gd ratio. When Nd/Gd ratio rises up, the increasing eutectics around the grain boundaries could not promote the hardness of the as-cast alloys, and number density of these crushed second phase in the extruded alloys increase. Nd/Gd ratio has little influence on the dynamic recrystallization process. The mechanical properties of the as-extruded alloys are not much decreasing with the increasing Nd/Gd ratio. The extruded Mg-6Gd-3Y-6Nd-0.6Zr has the best mechanical properties and lowest Gd addtion, and its ultimate tensile strength, yield strength and elongation are 336 MPa, 300 MPa and 2.5%, respectively. It should be ascribed to the equal cumulative effect of solid solution strengthening and second phase strengthening.

Acknowledgements

This research was financially supported by National Basic Research Program of China (Grant No. 2013CB632203), the Liaoning Provincial Natural Science Foundation of China (Grant No. 201202072 and 2014028027), the Program for Liaoning Excellent Talents in University (Grant No. LJQ2012023), and the Fundamental Research Foundation of Central Universities (Grant Nos. N120509002 and N120309003).

Reference

1 Rokhlin L L, *Magnesium alloys containing rare earth metals: structure and properties*, (Taylor & Francis, London), 2003.
2 Bettles C J & Gibson M A, *Adv Eng Mater*, 5 (2003) 859-865.
3 Mordike B L & Ebert T, *Mater Sci Eng A*, 302 (2001) 37-45.
4 Gorsse S, Hutchinson C R, Chevalier B & Nie J F, *J Alloys Compd*, 392 (2005) 253-262.
5 NIE. J F & Muddle C, *Acta Mater*, 48 (2000) 1691-1703.
6 Zou H, Zeng X, Zhai C & Ding W, *Mater Sci Eng A*, 402 (2005) 142-148.
7 Anyanwu I A, Kamado S & Kojima Y, *Mater Trans*, 42 (2001) 1212-1218.
8 Wang R, Dong J, Fan L-K, Zhang P & Ding W-J, *Trans. Nonferrous. Met. Soc. China*, 18, Supplement 1 (2008) s189-s193.
9 Li R G, Nie J F, Huang G J, Xin Y C & Liu Q, *Scr Mater*, 64 (2011) 950-953.
10 Vostrý P, Smola B, Stulikova I, Von Buch F & Mordike B, *Phys Stat Solidi (a)*, 175 (1999) 491-500.
11 Leontis T E, *Trans Am Inst Min Metall Eng*, 185 (1949) 968 - 983.
12 Peng Q, Wu Y, Fang D, Meng J & Wang L, *J Mater Sci*, 42 (2007) 3908-3913.
13 Negishi Y, Nishimura T, Iwasawa S, Kamado S, Kojima Y & Ninomiya R, *J Jpn I Light Met*, 44 (1994) 549-551.
14 Peng Q M, Wu Y M, Fang D Q, Meng J & Wang L M, *J. Alloys Compd*, 430 (2007) 252-256.
15 Wang J, Meng J, Zhang D & Tang D, *Mater Sci Eng A*, 456 (2007) 78-84.
16 Hou X, Cao Z, Sun X, Wang L & Wang L, *J Alloys Compd*, 525 (2012) 103-109.
17 Peng Q, Wang J, Wu Y & Wang L, *Mater Sci Eng A*, 433 (2006) 133-138.
18 Kleiner S, Beffort O, Wahlen A & Uggowitzer P J, *J Light Met*, 2 (2002) 277-280.
19 Lyakyshev N P, *Diagrams of binary metal systems*, 1996.
20 Lukac P, *Int Magnesium Conf*, 3 rd, UMIST, Manchester, United Kingdom, 1997, pp. 381-390.
21 Peng Q, Hou X, Wang L, Wu Y, Cao Z & Wang L, *Mater Des*, 30 (2009) 292-296.
22 Yu Z J, Huang Y, Qiu X, Yang Q, Sun W, Tian Z, Zhang D P & Meng J, *Mater Sci Eng A*, 578 (2013) 346-353.
23 Zheng K Y, Dong J, Zeng X Q & Ding W J, *Mater Sci Technol*, 24 (2008) 320-326.
24 He S M, Zeng X Q, Peng L M, Gao X, Nie J F & Ding W J, *J Alloys Compd*, 427 (2007) 316-323.
25 Gao Y, Wang Q, Gu J, Zhao Y & Tong Y, *Mater Sci Eng A*, 459 (2007) 117-123.
26 Sandlöbes S, Zaefferer S, Schestakow I, Yi S & Gonzalez-Martinez R, *Acta Mater*, 59 (2011) 429-439.
27 Goetz R, *Scr Mater*, 52 (2005) 851-856.
28 Xia X, Chen Q, Zhang K, Zhao Z, Ma M, Li X & Li Y, *Mater Sci Eng A*, 587 (2013) 283-290.
29 Robson J D, Henry D T & Davis B, *Acta Mater*, 57 (2009) 2739-2747.
30 Peng T, Wang Q, Lin J, Liu M & Roven H J, *Mater Sci Eng A*, 528 (2011) 1143-1148.
31 Xia X, Zhang K, Li X, Ma M & Li Y, *Mater Des*, 44 (2013) 521-527.
32 Li T, Zhang K, Li X, Du Z, Li Y, Ma M & Shi G, *J Magnes Alloy*, 1 (2013) 47-53.
33 Máthis K, Gubicza J & Nam N, *J Alloys Compd*, 394 (2005) 194-199.
34 Su J, Kaboli S, Kabir A S H, Jung I-H & Yue S, *Mater Sci Eng A*, 587 (2013) 27-35.